J. Phys. Earth, **25**, 117-142, 1977

AMPLITUDES OF THE EARTH'S SPLIT NORMAL MODES

Seth STEIN and Robert J. GELLER

Seismological Laboratory, California Institute of Technology
Pasadena, California, U.S.A.

(Received January 10, 1977)

This paper develops the theory necessary to explain the amplitudes of the earth's split normal modes. Expressions are derived for the amplitudes of the free oscillations of a laterally homogeneous rotating and elliptical earth excited by a point double couple. The eigenfunctions for this problem are the complex vector spherical harmonics about the north pole. The amplitudes of the normal modes are obtained by transforming SAITO's (1967) results, expressed in vector spherical harmonics about the earthquake source, into geographic coordinates. We explicitly show the dependence of the excitation of each singlet within a multiplet on geometric fault parameters, seismic moment, source depth, earth structure and the geographic coordinates of the source and receiver. We present synthetic torsional and spheroidal displacement and strain spectra for low order fundamental modes (${}_0S_2$-${}_0S_5$, ${}_0T_2$-${}_0T_5$) excited by four basic fault geometries.

Our results are suitable for the synthesis of observed spectra and time domain records in which splitting is an important effect. We have applied these results elsewhere to the Chilean and Alaskan earthquakes and have obtained very good agreement with observations.

1. *Introduction*

Following the observation of split peaks with varying amplitudes in the free oscillation spectra of the 1960 Chilean earthquake (by NESS *et al.*, 1961 and BENIOFF *et al.*, 1961), PEKERIS *et al.* (1961) and BACKUS and GILBERT (1961) showed that the splitting could be explained by the earth's rotation. Pekeris *et al.* and Backus and Gilbert calculated the relative amplitudes of the low order spheroidal modes excited by several simple sources. In this paper we calculate the amplitudes of the split modes of a rotating and elliptical earth due to a realistic model of an earthquake source, a double couple of arbitrary orientation.

Our results for the excitation of the split modes allow us to use the relative amplitudes of singlets to study earthquake source mechanisms. Recently (GELLER and STEIN, 1977) we have calculated for the first time the theoretical singlet amplitude ratios from published source parameters for the 1960 Chilean

earthquake and the 1964 Alaskan earthquake. For both events our synthetic relative spectral amplitudes are in remarkable agreement with observations of very low order modes. We are also able to analyze several hundred hours of records from the Chilean earthquake for these low order modes. These records are dominated by a complicated signal generated by rotational splitting which we are able to match quite closely (STEIN and GELLER, 1977) using the results we derive here.

The calculation of the excitation of the normal modes of a nonrotating, laterally homogeneous earth is greatly simplified by its spherical symmetry. As a result of the degeneracy arising from this symmetry, vector spherical harmonics in coordinates with the source on the polar axis may be chosen as eigenfunctions. This choice greatly simplifies the excitation calculations, because the eigenfrequency depends only on the angular order number, l, and only modes with azimuthal order numbers $m=0, \pm 1, \pm 2$ are excited by a point double couple.

The earth's rotation and ellipticity remove the degeneracy of the problem. For the nondegenerate problem, splitting is caused by the perturbing effects of the Coriolis force, centripetal force and ellipticity, all of which are symmetric about the earth's rotation axis. In contrast to the degenerate case, there is a distinct eigenfrequency, ω_{lm}, for each singlet. DAHLEN (1968) showed that the zeroeth order eigenfunctions are complex vector spherical harmonics about the North Pole, and calculated the eigenfrequencies of the split modes for several earth models. Although the frequency splitting within a multiplet depends on the earth's rotation rate, ellipticity and structure, the zeroeth order *amplitudes* of the split normal modes do *not* depend on the rotation rate and the ellipticity, and may thus be calculated without taking into account the precise frequency separation.

A substantial portion of the method for calculating the excitation of the degenerate modes may be adapted to the nondegenerate case, although much additional complexity results because the source is not on the axis of symmetry. The most important consequence of the removal of the degeneracy is that in general, for a double couple point source, modes of every azimuthal order number from $m=-l$ to $m=+l$ are excited. We show that the spectral amplitudes of the pair of singlets of orders m are equal. Furthermore, the geographic coordinates of the source and receiver appear individually in our expressions for the amplitudes, while for the degenerate case only their relative position affects the final result.

If the additional perturbation induced by lateral heterogeneity is introduced, then in general the eigenfunctions are linear combinations of the spherical harmonics (SAITO, 1971; USAMI, 1971; MADARIAGA, 1972; MADARIAGA and AKI, 1972; LUH, 1974). In this study we consider only the effects of

rotation and ellipticity which are the primary causes of the splitting of the low order modes. In the remainder of this paper we use *nondegenerate* to denote the case of a laterally homogeneous, rotating and elliptical earth, which has complete symmetry about the rotation axis.

Many authors have considered the excitation of the earth's normal modes. SAITO (1967) presented expressions for the excitation of free oscillations by a point source in a spherically symmetric earth. KANAMORI (1970a, b, 1971, 1976), ABE (1970), FUKAO and ABE (1971), SHIMAZAKI (1975), OKAL (1976), and other authors applied Saito's normal mode results to the synthesis of long period surface waves. KANAMORI and CIPAR (1974) presented compact expressions for the excitation problem. GILBERT (1970) introduced the moment tensor representation of a seismic source, which is formally equivalent to the double couples and couples without moment used by SAITO (1967) and TAKEUCHI and SAITO (1972). The equivalence has been discussed by several authors, e.g. GELLER (1976). LUH and DZIEWONSKI (1976) modified the moment tensor solution to include the effects of rotation and ellipticity.

In this paper we extend Saito's results to obtain the excitation of the nondegenerate normal modes. Our approach allows us to apply solutions for the excitation of degenerate normal modes (Saito, Kanamori and Cipar) to the nondegenerate modes. We derive expressions for torsional and spheroidal displacement and strain fields in the time domain. These expressions may then be used to calculate spectral amplitudes.

We calculate synthetic displacement and strain spectra for low order fundamental mode torsional and spheroidal multiplets (angular orders two through five) excited by four basic fault geometries (vertical and 45° dip; pure dip slip and strike slip). For particular source and receiver locations we present figures showing the relative spectral amplitudes of the individual singlets within each multiplet for each displacement and strain component. In general, the relative amplitudes within a multiplet will vary substantially with angular order number or even between different displacement or strain components for the same order number. Usually there is no consistency in the preferential excitation of singlet pairs with azimuthal order numbers $\pm m$ between multiplets.

Our method may be summarized as follows. We use DAHLEN's (1968) results for the case of complete symmetry about the rotation axis. Since the zeroeth order eigenfunctions are the complex vector spherical harmonics about the north pole, we obtain the excitation in terms of these eigenfunctions. To do so we use the rotation matrix elements to transform the excitation expanded in vector spherical harmonics about the source into the geographic coordinates.

This first order perturbation theory using zeroeth order eigenfunctions and first order eigenfrequencies is, of course, an approximation. Such an

approximation, in which the eigenvalue is found to a higher order than the eigenfunction, is a common practice in applications of perturbation theory. We regard the resulting zeroeth order amplitudes as being adequate for our purposes, as our intent is to derive results suitable for comparison to observations. For this purpose we require far greater precision in the eigenfrequency than in the eigenfunction.

By examining spectra, eigenfrequencies can be determined quite precisely. On the other hand, spectral amplitudes cannot be measured very precisely; the uncertainty is probably at least 10%. Since the error made in omitting the first order correction to the eigenfunctions is of the same order as the first order correction to the eigenfrequencies, and is almost certainly smaller than the experimental uncertainty in the amplitudes, it seems sufficient to use the zeroeth order amplitudes. Similarly, the first order eigenfrequencies seem acceptable in view of present experimental errors.

The true test of such an approximation is in its application to the data. Because we are successful in synthesizing spectra (GELLER and STEIN, 1977) and time domain records (STEIN and GELLER, 1977) it appears that the first order perturbation theory is all that we require.

Our method, using the rotation matrix elements, could also be generalized to the case of a laterally heterogeneous earth. Since the eigenfunctions are now linear combinations of the spherical harmonics about the north pole (LUH, 1974), we would again transform the excitation into the geographic coordinates. The final result would then be obtained by taking the appropriate linear combinations. Due to the complexity of this procedure and our ability to fit data for very low order modes with a model including only rotation and ellipticity, we do not include the effect of lateral heterogeneity in this paper.

2. *Normal Modes of a Rotating Elliptical Earth*

We adapt SAITO's (1967) results for the normal modes of a spherically symmetric earth to the case of a laterally homogeneous, rotating and elliptical earth. The displacements and stresses are expanded in complex vector spherical harmonics about the north pole.

The torsional and spheroidal displacements are respectively

$$\boldsymbol{U}^T(\boldsymbol{r}, t)=\sum_{n=0}^{\infty}\sum_{l=0}^{\infty}\sum_{m=-l}^{l} {}_nA_{lm}\boldsymbol{T}_{lm}(\theta, \phi)_n[y_1^T(r)]_{lm}(e^{i\,{}_n\omega_{lm}^{+}t}+e^{i\,{}_n\omega_{lm}^{-}t}) \tag{2.1}$$

and

$$\boldsymbol{U}^S(\boldsymbol{r}, t)=\sum_{n=0}^{\infty}\sum_{l=0}^{\infty}\sum_{m=-l}^{l} {}_nD_{lm}\{{}_n[y_1^S(r)]_{lm}\boldsymbol{S}_{lm}^1(\theta, \phi)+{}_n[y_3^S(r)]_{lm}\boldsymbol{S}_{lm}^2(\theta, \phi)\} \times(e^{i\,{}_n\omega_{lm}^{+}t}+e^{i\,{}_n\omega_{lm}^{-}t})\,. \tag{2.2}$$

The torsional and spheroidal vertical stresses, $\boldsymbol{P}=(P_{rr}, P_{r\theta}, P_{r\phi})$ are

$$\boldsymbol{P}^T(\boldsymbol{r}, t)=\sum_{n=0}^{\infty}\sum_{l=0}^{\infty}\sum_{m=-l}^{l} {}_nA_{lm}\boldsymbol{T}_{lm}(\theta, \phi)_n[{}_nV_2^T(r)]_{lm}(e^{i\,{}_n\omega_{lm}^{+}t}+e^{i\,{}_n\omega_{lm}^{-}t}) \tag{2.3}$$

and

$$\boldsymbol{P}^S(\boldsymbol{r}, t)=\sum_{n=0}^{\infty}\sum_{l=0}^{\infty}\sum_{m=-l}^{l} {}_nD_{lm}\{{}_n[{}_nV_2^S(r)]_{lm}\boldsymbol{S}_{lm}^1(\theta, \phi)+{}_n[{}_nV_4^S(r)]_{lm}\boldsymbol{S}_{lm}^2(\theta, \phi)\}$$
$$\times(e^{i\,{}_n\omega_{lm}^{+}t}+e^{i\,{}_n\omega_{lm}^{-}t})\,. \tag{2.4}$$

We follow established usage, and denote eigenfrequencies for both torsional and spheroidal modes by ${}_n\omega_{lm}$, although the torsional eigenfrequencies (in 2.1) and (2.3) differ from the spheroidal ones (in (2.2) and (2.4)). The frequency in question should be clear from the context.

For the degenerate problem, each mode has two eigenfrequencies with equal absolute value, but opposite sign. However, when a perturbation is applied, the eigenfrequencies associated with a particular mode no longer have the same absolute value. The positive eigenfrequencies (${}_n\omega_{lm}^{+}$) may be considered as the "physical" frequencies of the split modes. The negative eigenfrequencies (${}_n\omega_{lm}^{-}$) arise from any application of perturbation theory to the splitting problem (e.g. BACKUS and GILBERT, 1961). In later sections the negative eigenfrequencies will be eliminated from the final expressions.

The sum over n sums all the overtones. From this point we consider only a single overtone and suppress the sum over n and all overtone indices. The complete displacement and stress fields can always be derived by adding all the overtones.

A_{lm} and D_{lm} are the amplitudes of the individual spheroidal and torsional modes and are found by solving the excitation problem. $[{}_nV_l^S]_{lm}$ and $[{}_nV_l^T]_{lm}$ are the spheroidal and torsional radial eigenfunctions. Though derived for the degenerate case, they remain valid, to zeroeth order, for the nondegenerate case. Following ALTERMAN *et al.* (1959) and SAITO (1967) we will suppress all subscripts on the $[{}_nV_l]_{lm}$ in the remainder of the paper.

The surficial basis vectors for the normal mode expansions are the complex vector spherical harmonics

$$\boldsymbol{T}_{lm}(\theta, \phi)=\left(0, \frac{1}{\sin\theta}\frac{\partial Y_{lm}(\theta, \phi)}{\partial\phi}, -\frac{\partial Y_{lm}(\theta, \phi)}{\partial\theta}\right)$$
$$\boldsymbol{S}_{lm}^1(\theta, \phi)=(Y_{lm}(\theta, \phi), 0, 0) \tag{2.5}$$
$$\boldsymbol{S}_{lm}^2(\theta, \phi)=\left(0, \frac{\partial Y_{lm}(\theta, \phi)}{\partial\theta}, \frac{1}{\sin\theta}\frac{\partial Y_{lm}(\theta, \phi)}{\partial\phi}\right)$$

where

$$Y_{lm}(\theta, \phi)=(-1)^m\left[\frac{(l-m)!}{(l+m)!}\right]^{1/2}P_l^m(\cos\theta)e^{im\phi}\quad(m\geq 0) \tag{2.6}$$

and

$$Y_{lm}(\theta, \phi)=(-1)^mY_{l,-m}^*(\theta, \phi)\quad(m<0)$$

θ is the colatitude and ϕ is the longitude. * denotes complex conjugate. The associated Legendre polynomials are defined as

$$P_l^m(x)=(1-x^2)^{m/2}\frac{d^m}{dx^m}P_l(x)\,. \tag{2.7}$$

The vector spherical harmonics then have the orthogonality and normalization properties

$$\begin{aligned}\int_0^{2\pi}\int_0^{\pi}(\boldsymbol{T}^*_{l'm'}(\theta,\phi))\cdot(\boldsymbol{T}_{lm}(\theta,\phi))\sin\theta d\theta d\phi&\\ =L^2\int_0^{2\pi}\int_0^{\pi}(\boldsymbol{S}^{1*}_{l'm'}(\theta,\phi))\cdot(\boldsymbol{S}^{1}_{lm}(\theta,\phi))\sin\theta d\theta d\phi&\\ =\int_0^{2\pi}\int_0^{\pi}(\boldsymbol{S}^{2*}_{l'm'}(\theta,\phi))\cdot(\boldsymbol{S}^{2}_{lm}(\theta,\phi))\sin\theta d\theta d\theta&\\ =\frac{4\pi L^2}{2l+1}\delta_{ll'}\delta_{mm'}&\end{aligned} \tag{2.8}$$

where

$$L^2=l(l+1)$$

and

$$\delta_{mm'}=\begin{cases}0 & m\neq m'\\ 1 & m=m'\,.\end{cases}$$

Equation (2.6) gives us the symmetry relations

$$\begin{aligned}\boldsymbol{T}_{lm}(\theta,\phi)&=(-1)^m\boldsymbol{T}^*_{l,-m}(\theta,\phi)\\ \boldsymbol{S}^1_{lm}(\theta,\phi)&=(-1)^m\boldsymbol{S}^{1*}_{l,-m}(\theta,\phi)\\ \boldsymbol{S}^2_{lm}(\theta,\phi)&=(-1)^m\boldsymbol{S}^{2*}_{l,-m}(\theta,\phi)\end{aligned} \tag{2.9}$$

for the vector spherical harmonics.

DAHLEN (1968) applied perturbation theory to the degenerate case, and calculated the splitting for several earth models. The perturbed eigenfrequencies may be found from the unperturbed eigenfrequency, using

$$\omega_{lm}=\omega_l+(\delta\omega)_{lm}\,. \tag{2.10}$$

Here the perturbed eigenfrequency, ω_{lm}, and the unperturbed eigenfrequency, ω_l, may be either positive or negative but must have the same sign. The frequency shift $(\delta\omega)$ is given by

$$(\delta\omega)_{lm}=\omega_l(\alpha_l+m\beta_l+m^2\gamma_l) \tag{2.11}$$

in Dahlen's notation, where the splitting parameters α_l and γ_l are due to the ellipticity, and β_l is due to the earth's rotation. Because of the m^2 dependence of $(\delta\omega)_{lm}$, the perturbed eigenfrequencies are not symmetrically spaced about the unperturbed eigenfrequency or the central perturbed frequency.

The splitting parameters for positive and negative frequencies are related by

$$\begin{aligned} \alpha_l(\omega_l^+) &= \alpha_l(\omega_l^-) \\ \beta_l(\omega_l^+) &= -\beta_l(\omega_l^-) \\ \gamma_l(\omega_l^+) &= \gamma_l(\omega_l^-) \,. \end{aligned} \tag{2.12}$$

Since $\omega_l^+ = -\omega_l^-$, (2.11) and (2.12) show that

$$(\delta\omega)_{lm}^+ = -(\delta\omega)_{l,-m}^- \tag{2.13}$$

and thus

$$\omega_{lm}^+ = -\omega_{l,-m}^- \tag{2.14}$$

but in general $|\omega_{lm}^+| \neq |\omega_{lm}^-|$.

We will use (2.14), together with the symmetry relations between spherical harmonics (2.9), to eliminate the negative eigenfrequencies from the expressions in sections 4 and 5.

3. *Transformation of the Source Discontinuities into Geographic Coordinates*

We now generalize SAITO's (1967) results to the case of a rotating, elliptical earth. A point source causes discontinuities in stress and displacement across an infinitesimal shell, which are expanded in vector spherical harmonics. The expansion coefficients are required to find the amplitudes of the free oscillations. For the nondegenerate case, the expansion must be carried out in the geographic coordinate frame. LUH and DZIEWONSKI (1976) calculate these expansion coefficients from scratch for each individual source location and mechanism.

Our approach is to use Saito's expansion coefficients for the discontinuities resulting from a double couple, in a coordinate system with the source on the polar axis. We then use elements of the rotation matrices to transform this spherical harmonic expansion into the geographic coordinate frame. Thus for any source location we perform a simple transformation rather than completely recalculate the expansion coefficients.

It is first necessary to introduce the coordinate system of the earthquake source, and to show how the rotation matrix elements allow us to transform the expansion coefficients from this coordinate system to the geographic system.

We adopt the fault geometry of Kanamori and Cipar, shown in Fig. 1. We use a coordinate system in which the source is at ($r=r_s$, $\theta'=0$, $\phi'=0$) and describe points in this system by (r, θ', ϕ'). In this frame the fault strike, at an angle ρ measured counterclockwise from north, is the X_1' axis. The X_3' axis is vertical. The fault plane dips at an angle δ measured from the negative X_2' axis, and the slip angle λ, which gives the direction in which the hanging wall

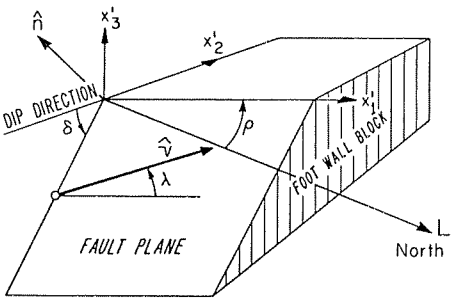

Fig. 1. Fault representation of Kanamori and Cipar (slightly modified). $\hat{v}$ is the slip vector, and gives the displacement of the hanging wall block. $\hat{n}$ is the normal to the fault plane, and L points north. The strike ρ is measured counterclockwise from L. The dip angle δ is measured from the negative X'_2 axis, and the slip angle λ is measured in the fault plane counterclockwise from X'_1.

block moves with respect to the foot wall, is measured counterclockwise from X'_1 in the fault plane. The cartesian unit vector in the direction of slip is given by

$$\hat{v}=(\cos\lambda,\ \sin\lambda\cos\delta,\ \sin\lambda\sin\delta) \tag{3.1}$$

and the unit normal to the fault plane is

$$\hat{n}=(0,\ -\sin\delta,\ \cos\delta)\ . \tag{3.2}$$

The geographic coordinates of the source are $(r_s,\ \theta_s,\ \phi_s)$, and points in the geographic system have coordinates $(r,\ \theta,\ \phi)$. The X_3 axis is the polar axis and the X_1–X_3 plane is the plane of the prime meridian. Thus the unit vector $\hat{\theta}$ points south at any point and $\hat{\phi}$ points east.

Hereafter, we will use primes $(X'_i,\ f'_i,\ y'_i,\ A'_{lm})$ to denote quantities associated with the source coordinate frame. The corresponding unprimed quantities are associated with the geographic coordinates.

The source and geographic systems can be related to each other through the three Euler angles which allow us to rotate the geographic $(X_1,\ X_2,\ X_3)$ axes into the source $(X'_1,\ X'_2,\ X'_3)$ axes. To perform this transformation we start with the $X_1,\ X_2,\ X_3$ axes and make three counterclockwise rotations. We first rotate by α about the X_3 axis, then by β about the resulting X_2 (or X_2^*) axis, and finally by γ about the X'_3 axis. This process is shown in Fig. 2. The line L, drawn to clarify the choice of Euler angles, points north in the X'_1–X'_2 plane. We see that for a source at $\theta_s,\ \phi_s$, with fault strike ρ,

$$\alpha=\phi_s\ ,\qquad \beta=\theta_s\ ,\qquad \gamma=\pi+\rho\ . \tag{3.3}$$

(This is only true for the Euler angle conventions of BRINK and SATCHLER (1968)—at least three other conventions are used by other authors.)

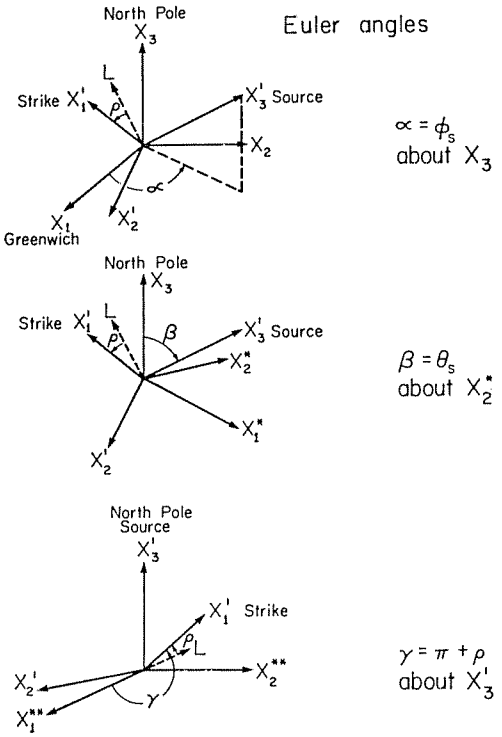

Fig. 2. Euler angles which rotate geographic (X_1, X_2, X_3) axes into source (X_1', X_2', X_3') axes. All rotations are right handed. The line L points north in the X_1'-X_2' plane.

Brink and Satchler show that spherical harmonics in the two coordinate systems are related by the rotation matrices $\mathscr{D}^l_{mk}(\alpha, \beta, \gamma)$ which are irreducible representations of the rotation group. For brevity, we will denote this set of three Euler angles by $R=(\alpha, \beta, \gamma)$. The rotation matrix elements are then given by

$$\mathscr{D}^l_{mk}(R)=e^{-i(\alpha m+\gamma k)}d^l_{mk}(\beta) \tag{3.4}$$

where

$$d^l_{mk}(\beta)=\sum_t (-1)^t \frac{[(l+m)!(l-m)!(l+k)!(l-k)!]^{1/2}}{t!(l+m-t)!(l-k-t)!(t+k-m)!} \times[\sin(\beta/2)]^{2t+k-m}[\cos(\beta/2)]^{2l+m-k-2t} \tag{3.5}$$

and the summation ranges over all values of t which give non-negative factorials. Derivations of the rotation matrix elements are also given by Satô (1950).

The relation between spherical harmonics in the source and geographic frames is then

$$Y_{lk}(\theta', \phi')=\sum_{m=-l}^{l} \mathscr{D}^l_{mk}(R)Y_{lm}(\theta, \phi)\,. \tag{3.6}$$

Since the vector spherical harmonics are themselves vectors, we may write equalities between vectors (rather than their components)

$$\begin{aligned} \boldsymbol{T}_{lk}(\theta', \phi') &= \sum_{m=-l}^{l} \mathscr{D}^{l}_{mk}(R)\boldsymbol{T}_{lm}(\theta, \phi) \\ \boldsymbol{S}^{1}_{lk}(\theta', \phi') &= \sum_{m=-l}^{l} \mathscr{D}^{l}_{mk}(R)\boldsymbol{S}^{1}_{lm}(\theta, \phi) \\ \boldsymbol{S}^{2}_{lk}(\theta', \phi') &= \sum_{m=-l}^{l} \mathscr{D}^{l}_{mk}(R)\boldsymbol{S}^{2}_{lm}(\theta, \phi) \,. \end{aligned} \tag{3.7}$$

(To compare individual components in (3.7) directly, the (θ, ϕ) components must be rotated into the (θ', ϕ') frame, or vice versa.)

We now use the rotation matrix elements to obtain the expansion in geographic coordinates of the discontinuities in displacement and stress caused by a point source. We begin with this expansion in the source coordinates, and derive the relations between the two expansions. These relations will allow us to convert Saito's source frame results to the geographic results we require.

In the source frame, Saito's expressions for the discontinuities in displacement and stress can be rewritten as

$$\begin{aligned} \delta\boldsymbol{U}(r_s; t) &= \boldsymbol{U}(r_s+\varepsilon, t) - \boldsymbol{U}(r_s-\varepsilon, t) \\ &= \frac{1}{2\pi}\int_{-\infty}^{\infty} \sum_{l=0}^{\infty} \sum_{m=-l}^{l} [g_1'^{T}(\omega)\boldsymbol{T}_{lm}(\theta', \phi') + g_1'^{S}(\omega)\boldsymbol{S}^{1}_{lm}(\theta', \phi') \\ &\quad + g_3'^{S}(\omega)\boldsymbol{S}^{2}_{lm}(\theta', \phi')]e^{i\omega t}d\omega \end{aligned} \tag{3.8}$$

and

$$\begin{aligned} \delta\boldsymbol{P}(r_s; t) &= \boldsymbol{P}(r_s+\varepsilon, t) - \boldsymbol{P}(r_s-\varepsilon, t) \\ &= \frac{1}{2\pi}\int_{-\infty}^{\infty} \sum_{l=0}^{\infty} \sum_{m=-l}^{l} [g_2'^{T}(\omega)\boldsymbol{T}_{lm}(\theta', \phi') + g_2'^{S}(\omega)\boldsymbol{S}^{1}_{lm}(\theta', \phi') \\ &\quad + g_4'^{S}(\omega)\boldsymbol{S}^{2}_{lm}(\theta', \phi')]e^{i\omega t}d\omega \end{aligned} \tag{3.9}$$

where $\delta\boldsymbol{U}(r_s; t)$ and $\delta\boldsymbol{P}(r_s; t)$ are the jumps in displacement and stress respectively across a spherical shell at the source depth $r=r_s$.

For the special case of a step function source time dependence, the frequency dependent discontinuity coefficients $g_i'(\omega)$ may be written

$$g_i'(\omega) = \frac{(f_i)'}{i\omega} \tag{3.10}$$

where the f_i' are the expansion coefficients for the spatial dependence of the discontinuity. Each $(f_i^T)'$ or $(f_i^S)'$ has an implicit dependence on l and m.

To transform (3.8) and (3.9) to the geographic coordinates, we use the results derived in (3.7) for the vector spherical harmonics, and derive a general relation between the discontinuity expansion coefficients in geographic coordinates and those in source coordinates in terms of the rotation matrix elements

$$(f_i)_{lm} = \sum_{k=-l}^{l} \mathscr{D}^{l}_{mk}(R)(f_i)'_{lk} \,. \tag{3.11}$$

In this equation we have written the l, m dependence of the f_i explicitly. We will omit these subscripts in the remainder of our discussions. Note that, as the f_i are coefficients of the basis vectors, they transform, (3.11), in the opposite sense as the vector spherical harmonics (3.7).

Using this relation between the discontinuity expansion coefficients, we could rewrite (3.8) and (3.9) to obtain expressions for the discontinuities in displacement and stress in the geographic coordinates. We will not do so, because in calculating the excitation, we require the discontinuity expansion coefficients, f_i (3.11), rather than the discontinuities themselves.

4. *Torsional Modes Excited by a Point Double Couple*

We now use the expansion coefficients in geographic coordinates to apply Saito's excitation results to the nondegenerate case. We derive the excitation of the torsional modes in some detail in this section; we present results for spheroidal modes in the next section. It is shown that although (in source coordinates) only singlets of orders $m=-2$ through $m=+2$ are excited in the degenerate case, all $2l+1$ singlets within a multiplet are excited in the nondegenerate case.

We now modify Saito's results for the displacements resulting from a point source with step function time dependence and unit seismic moment. To zeroeth order, in the geographic frame, Saito's expression may be written as

$$\boldsymbol{U}^T(\boldsymbol{r}, t)=\sum_{l=0}^{\infty}\sum_{m=-l}^{l} A_{lm} y_1^T(r)\boldsymbol{T}_{lm}(\theta, \phi)[e^{i\omega_{lm}^{+}t}+e^{i\omega_{lm}^{-}t}]\,, \tag{4.1}$$

where $\boldsymbol{r}$ is the position of the receiver, $y_1^T(r)$ and $y_2^T(r)$ are the eigenfunctions for the torsional modes, and I_1^T is an energy integral defined by Saito. A_{lm} is the modal amplitude

$$A_{lm}=\frac{[r^2(f_2^T y_1^T(r)-f_1^T y_2^T(r))]_{r=r_s}}{2\omega_l^2 I_1^T}\,. \tag{4.2}$$

As we have shown, we can express this as

$$A_{lm}=\sum_{k=-l}^{l}\mathscr{D}^l{}_{mk}(R)A'_{lk} \tag{4.3}$$

where the source frame modal amplitude is

$$A'_{lk}=\frac{[r^2((f_2^T)' y_1^T(r)-(f_1^T)' y_2^T(r))]_{r=r_s}}{2\omega_l^2 I_1^T}\,. \tag{4.4}$$

These equations are valid for an arbitrary point source. Saito gives expressions for $(f_1^T)'$ and $(f_2^T)'$ for a double couple, in terms of the real spherical harmonics $(P_l^m(\cos\theta)\cos m\phi$ and $P_l^m(\sin\theta)\sin m\phi)$ and in terms of the cartesian

components of the unit slip vector, $\hat{\nu}$, and the unit normal to the fault plane, $\hat{n}$. These can be transformed into the coefficients of positive and negative complex spherical harmonics for the fault representation of Kanamori and Cipar. For the complex (but still completely unnormalized) spherical harmonics, $P_l^m(\cos\theta)e^{im\phi}$, the coefficients become

$$r_s^2(f_1^T)' = \frac{2l+1}{4\pi L^2}\frac{1}{\mu_s}\frac{1}{2}(-\sin\lambda\cos 2\delta \mp i\cos\lambda\cos\delta) \tag{4.5}$$

for $m=\pm 1$, and

$$r_s^2(f_2^T)' = \frac{2l+1}{4\pi L^2}\frac{1}{r_s}\frac{1}{2}(-\cos\lambda\sin\delta \pm i\sin\lambda\sin\delta\cos\delta) \tag{4.6}$$

for $m=\pm 2$. Both of these quantities are zero for $m=0$, and $|m|>2$. (μ_s is the rigidity at the source depth r_s.)

To convert these coefficients into the coefficients of our normalized complex spherical harmonics, we multiply by the conversion factors,

$$C_{lm} = \left[\frac{(l+m)!}{(l-m)!}\right]^{1/2}(-1)^m \quad \text{for } m\geq 0 \tag{4.7}$$

and

$$C_{lm} = C_{l,-m}(-1)^m \quad \text{for } m<0\,.$$

For convenience, we introduce the source amplitude factors defined by Kanamori and Cipar for the degenerate excitation problem

$$L_1 = \left(\frac{2l+1}{4\pi\omega_l^2 L^2 I_1^T}\right)\left(\frac{1}{\mu_s}\right)y_2^T(r_s) \tag{4.8}$$

and

$$L_2 = \left(\frac{2l+1}{4\pi\omega_l^2 L^2 I_1^T}\right)\left(\frac{1}{r_s}\right)y_1^T(r_s)\,.$$

We now calculate the source frame modal amplitude (4.4), A'_{lm}, which is zero for $|m|>2$. If the radiation pattern terms are expressed as

$$p_1 = \frac{1}{4}(-\sin\lambda\cos 2\delta - i\cos\lambda\cos\delta)$$

and

$$p_2 = \frac{1}{4}(-\cos\lambda\sin\delta + i\sin\lambda\sin\delta\cos\delta) \tag{4.9}$$

we can write

$$\begin{aligned} A'_{l2} &= L_2 p_2 C_{l2} \\ A'_{l1} &= L_1 p_1 C_{l1} \\ A'_{l0} &= 0 \\ A'_{l,-1} &= L_1 p_1^* C_{l,-1} \\ A'_{l,-2} &= L_2 p_2^* C_{l,-2}\,. \end{aligned} \tag{4.10}$$

Thus we have the symmetry relation

$$A'_{lm}=(-1)^m A'^{*}_{l,-m}\,. \tag{4.11}$$

Brink and Satchler give a symmetry relation for the $\mathscr{D}^l_{mk}$ functions,

$$\mathscr{D}^l_{mk}(R)=[\mathscr{D}^l_{-m,-k}(R)]^{*}(-1)^{m-k}\,. \tag{4.12}$$

Substituting (4.10) and (4.11) into (4.3), we find the same symmetry for the geographic modal amplitudes as for the source frame amplitudes

$$A_{lm}=(-1)^m A^{*}_{l,-m}\,. \tag{4.13}$$

We use (4.13) and the symmetry properties of the vector spherical harmonics (2.9) to eliminate the negative eigenfrequencies, ω^{-}_{lm}, from (4.1). Defining

$$\boldsymbol{B}_{lm}(\boldsymbol{r})=y^1_1(r)A_{lm}\boldsymbol{T}_{lm}(\theta,\phi)\,, \tag{4.14}$$

which do not depend on the eigenfrequencies, we obtain the torsional mode displacements resulting from a double couple point source with step function source time history:

$$\boldsymbol{U}^T(\boldsymbol{r},t)=\sum_{l=0}^{\infty}\sum_{m=-l}^{l}\{\boldsymbol{B}_{lm}(\boldsymbol{r})e^{i\omega_{lm}t}+\boldsymbol{B}^{*}_{lm}(\boldsymbol{r})e^{-i\omega_{lm}t}\}\,, \tag{4.15}$$

where ω_{lm} is the positive eigenfrequency.

We can also combine terms to write the displacements in terms of real quantities

$$\boldsymbol{U}^T(\boldsymbol{r},t)=\sum_{l=0}^{\infty}\sum_{m=-l}^{l}\{2Re(\boldsymbol{B}_{lm}(\boldsymbol{r}))\cos\omega_{lm}t-2Im(\boldsymbol{B}_{lm}(\boldsymbol{r}))\sin\omega_{lm}t\}\,. \tag{4.16}$$

The displacements from spatially finite sources, or those with more complicated time functions, may be derived from (4.15) or (4.16) by convolution. By performing the implied summation over the overtones (n) and the summations over l and m, we obtain the entire displacement field. By summing only over l and m we obtain a given overtone (e.g. the fundamental). We can also sum, for a given n and l, all $2l+1$ singlets of a multiplet (e.g. ${}_0S_2$). As shown in STEIN and GELLER (1977) the singlets interfere in the time domain to produce a complicated beat pattern.

5. *Spheroidal Modes Excited by a Point Double Couple*

To find the spheroidal mode solutions, we modify Saito's results for the displacements resulting from an arbitrary point source with step function time dependence and unit seismic moment. To zeroeth order, in the geographic frame, Saito's expression is

$$\boldsymbol{U}^S(\boldsymbol{r}, t)=\sum_{l=0}^{\infty}\sum_{m=-l}^{l} D_{lm}\{y_1^S(r)\boldsymbol{S}_{lm}^1(\theta, \phi)+y_3^S(r)\boldsymbol{S}_{lm}^2(\theta, \phi)\}[e^{i\omega_l^+ t}+e^{i\omega_l^- t}] \quad (5.1)$$

where

$$D_{lm}=\frac{[r^2(f_2^S y_1^S(r)-f_1^S y_2^S(r))+L^2r^2(f_4^S y_3^S(r)-f_3^S y_4^S(r))]_{r=r_s}}{2\omega_l^2(I_1^S+L^2I_2^S)}\,. \quad (5.2)$$

We relate the geographic and source frame modal amplitudes by

$$D_{lm}=\sum_{k=-2}^{2}\mathscr{D}_{mk}^l(R)D'_{lk}\,. \quad (5.3)$$

Thus in the source frame,

$$D'_{lk}=\frac{[r^2((f_2^S)'y_1^S(r)-(f_1^S)'y_2^S(r))+L^2r^2((f_4^S)'y_3^S(r)-(f_3^S)'y_4^S(r))]_{r=r_s}}{2\omega_l^2(I_1^S+L^2I_2^S)}\,. \quad (5.4)$$

I_1^S and I_2^S are energy integrals for the spheroidal modes, also defined by Saito.

As we did for the torsional modes, we convert Saito's expansion coefficients for a double couple to those of the normalized complex vector spherical harmonics. These expressions are simplified by introducing the amplitude factors K_0, K_1, K_2 of Kanamori and Cipar:

$$\begin{aligned}
K_0&=\left(\frac{2l+1}{4\pi\omega_l^2(I_1^S+L^2I_2^S)r_s}\right)\left(\frac{2(3\lambda_s+2\mu_s)}{\lambda_s+2\mu_s}\right)\left(y_1^S(r_s)-\frac{r_s}{3\lambda_s+2\mu_s}y_2^S(r_s)-\frac{L^2}{2}y_3^S(r_s)\right)\\
K_1&=\frac{2l+1}{4\pi\omega_l^2(I_1^S+L^2I_2^S)}\,\frac{y_4^S(r_s)}{\mu_s}\\
K_2&=\frac{2l+1}{4\pi\omega_l^2(I_1^S+L^2I_2^S)}\,\frac{y_3^S(r_s)}{r_s}\,,
\end{aligned} \quad (5.5)$$

where λ_s and μ_s are the elastic constants at the source depth.

Using these, and the radiation pattern terms

$$\begin{aligned}
q_0&=\frac{1}{2}\sin\lambda\sin\bar{\delta}\cos\bar{\delta}\\
q_1&=\frac{1}{4}(-\cos\lambda\cos\bar{\delta}+i\sin\lambda\cos 2\bar{\delta})\\
q_2&=\frac{1}{4}(-\sin\lambda\cos\bar{\delta}\sin\bar{\delta}-i\cos\lambda\sin\bar{\delta})
\end{aligned} \quad (5.6)$$

we can derive our final relations for the D'_{lm} (which are zero for $|m|>2$)

$$\begin{aligned}
D'_{l2}&=K_2q_2C_{l2}\\
D'_{l1}&=K_1q_1C_{l1}\\
D'_{l0}&=K_0q_0C_{l0}\\
D'_{l,-1}&=K_1q_1^*C_{l,-1}\\
D'_{l,-2}&=K_2q_2^*C_{l,-2}\,.
\end{aligned} \quad (5.7)$$

Again, note that $D'_{lm}=(-1)^m D^*_{l-m}$. Thus for the geographic expansion coefficients

$$D_{lm}=(-1)^m D^*_{l,-m}\,. \tag{5.8}$$

To obtain our final results for the displacements, we define

$$\boldsymbol{E}_{lm}(\boldsymbol{r})=D_{lm}\{y_1^S(r)\boldsymbol{S}^1_{lm}(\theta,\phi)+y_3^S(r)\boldsymbol{S}^2_{lm}(\theta,\phi)\} \tag{5.9}$$

which do not depend on the eigenfrequencies. We can then write (after disposing of the negative frequencies) that

$$\boldsymbol{U}^S(\boldsymbol{r},t)=\sum_{l=0}^{\infty}\sum_{m=-l}^{l}\{\boldsymbol{E}_{lm}(\boldsymbol{r})e^{i\omega_{lm}t}+\boldsymbol{E}^*_{lm}(\boldsymbol{r})e^{-i\omega_{lm}t}\} \tag{5.10}$$

or

$$\boldsymbol{U}^S(\boldsymbol{r},t)=\sum_{l=0}^{\infty}\sum_{m=-l}^{l}\{2Re(\boldsymbol{E}_{lm}(r))\cos\omega_{lm}t-2Im(\boldsymbol{E}_{lm}(r))\sin\omega_{lm}t\}\,. \tag{5.11}$$

Note that (5.11) shows that the displacements are real. As with the torsional modes, ω_{lm} is the positive eigenfrequency.

For an isotropic source of unit moment (5.1) through (5.4), (5.10) and (5.11) are used, but the only nonzero excitation coefficient in the source frame is

$$D'_{l0}=K'_0C_{l0} \tag{5.12}$$

where the source amplitude factor K'_0 is adapted from TAKEUCHI and SAITO (1972)

$$K'_0=\frac{2l+1}{4\pi\omega_l^2(I_1+L^2I_2)}\left[-\frac{4\mu_s}{(\lambda_s+2\mu_s)}\frac{y_1^S(r_s)}{r_s}-\frac{y_2^S(r_s)}{(\lambda_s+2\mu_s)}+\frac{2L^2\mu_s y_3^S(r_s)}{(\lambda_s+2\mu_s)r_s}\right]. \tag{5.13}$$

6. *Numerical Results*

The final expressions for the displacements of spheroidal (5.11) and torsional (4.16) modes are suitable for numerical computation. We require only the source amplitude factors K_0, K_1, K_2, L_1 and L_2, the radial eigenfunctions $y_i(r)$, the three geometric fault parameters (strike, dip and slip), the locations of the source and receiver and the seismic moment. We investigate the dependence of the displacement and strain spectra of the fundamental torsional and spheroidal modes on the geometric fault parameters and the positions of the source and receiver. This also provides us with a method of checking our results. We ensure that the total of the displacements and strains within each multiplet at time $t=0$ are equal to those calculated from the expressions of KANAMORI and CIPAR (1974) for the degenerate modes. A second test is to verify that for an isotropic source we derive the same results from the addition theorem for Legendre polynomials (PEKERIS *et al.*, 1961).

Table 1. Source amplitude factors and surface eigenfunctions.

Mode	K_0	K_1	K_2	$y_1^S(a)$ (cm)	$y_3^S(a)$ (cm)
${}_0S_2$	$.616\times10^{-3}$	$.209\times10^{-5}$	$.678\times10^{-5}$	1.	$.252\times10^{-1}$
${}_0S_3$	$.773\times10^{-3}$	$.245\times10^{-5}$	$-.160\times10^{-4}$	1.	$-.124$
${}_0S_4$	$.768\times10^{-3}$	$.243\times10^{-5}$	$-.137\times10^{-4}$	1.	$-.150$
${}_0S_5$	$.760\times10^{-3}$	$.204\times10^{-5}$	$-.105\times10^{-4}$	1.	$-.146$

Mode	L_1	L_2	$y_1^T(a)$ (cm)
${}_0T_2$	$.493\times10^{-5}$	$.987\times10^{-4}$	1.
${}_0T_3$	$.391\times10^{-5}$	$.337\times10^{-4}$	1.
${}_0T_4$	$.341\times10^{-5}$	$.178\times10^{-4}$	1.
${}_0T_5$	$.308\times10^{-5}$	$.114\times10^{-4}$	1.

The values of the source amplitude factors K_0, K_1, K_2 and L_1, L_2, which were used by Kanamori and Cipar are listed in Table 1. These amplitude factors are for a hypocentral depth of 55 km and a moment of 10^{27} dyne-cm. We also list the radial displacement eigenfunctions at the earth's surface ($r=a$) for each mode. $y_1^T(a)$ and $y_1^S(a)$ are normalized to one; only $y_3^S(a)$ varies from mode to mode.

We also require the radiation pattern coefficients, which are given in Table 2 for each of the four basic faults. For the degenerate case, q_0 is the coefficient for radially symmetric Rayleigh waves; q_1 and p_1, for two-lobed Rayleigh and Love waves and q_2 and p_2, for a four-lobed radiation pattern. Seismologists have developed considerable intuition in using surface wave radiation patterns to find fault geometries. It is much more difficult to interpret the singlet amplitudes in our figures intuitively, because each singlet amplitude involves a sum, (4.3) or (5.3), of source frame amplitudes weighted by the rotation matrix elements. Thus, except for some special cases, it is difficult to find simple explanations of the relative amplitudes of singlets within a multiplet.

Strain and displacement spectra are calculated for eight fundamental low order number modes: ${}_0S_2$–${}_0S_5$ and ${}_0T_2$–${}_0T_5$. These modes were chosen because

Table 2. Source frame radiation pattern terms.

Fault Type	λ	δ	q_0	q_1	q_2	p_1	p_2
Vertical dip slip (Figs. 3 & 8)	90°	90°	0	$-\frac{i}{4}$	0	$\frac{1}{4}$	0
Vertical strike slip (Figs. 4 & 9)	0°	90°	0	0	$-\frac{i}{4}$	0	$-\frac{1}{4}$
45° dipping dip slip (Figs. 5 & 10)	90°	45°	$\frac{1}{4}$	0	$-\frac{1}{8}$	0	$\frac{i}{8}$
45° dipping strike slip (Figs. 6 & 11)	0°	45°	0	$-\frac{1}{4\sqrt{2}}$	$-\frac{i}{4\sqrt{2}}$	$-\frac{i}{4\sqrt{2}}$	$-\frac{1}{4\sqrt{2}}$

it appears almost certain that they are not seriously affected by perturbations resulting from lateral inhomogeneities. Furthermore, it is only for the lowest order modes that individual singlet peaks have definitely been resolved observationally.

In Figs. 3–6 we show synthetic line spectra for four fundamental spheroidal modes. For graphical purposes the lines are drawn symmetrically and evenly spaced about the central frequency, although the eigenfrequency spacing is in fact uneven and asymmetric. The effect of attenuation in broadening these lines has not been included. Amplitudes are normalized within each displacement and strain component.

We plot the spectral amplitude (the modulus of the appropriate l, m component of $\boldsymbol{E}_{lm}$) of each displacement and horizontal strain. Note that the

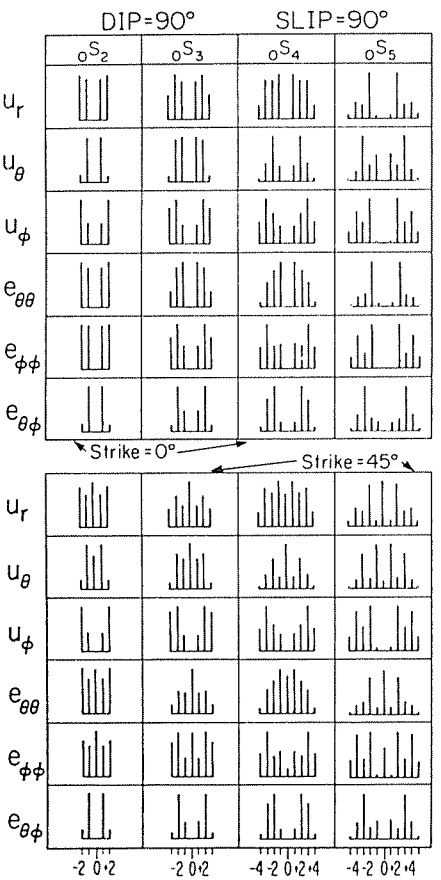

Fig. 3. Spheroidal mode amplitude spectra for a vertical dip slip fault at $\theta_s=30°$, $\phi_s=0°$ observed at $\theta=105°$, $\phi=120°$ for $\rho=0°$ and $\rho=45°$.

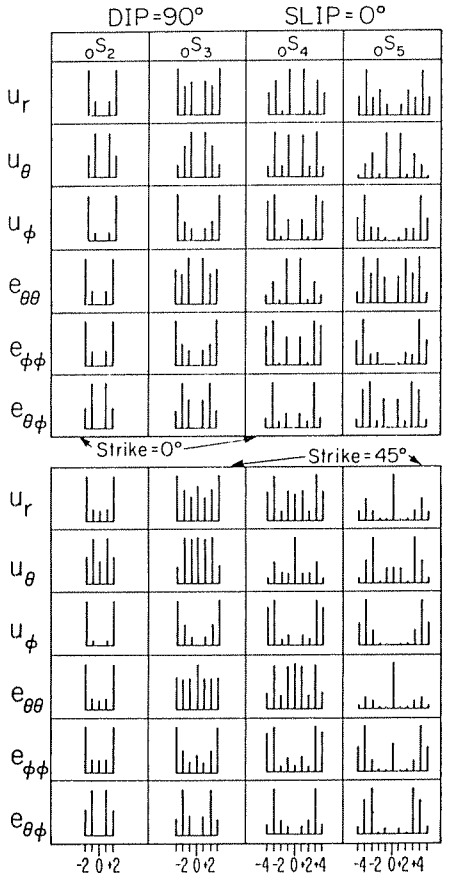

Fig. 4. Spheroidal mode amplitude spectra for a vertical strike slip fault at $\theta_s=30°$, $\phi_s=0°$ observed at $\theta=105°$, $\phi=120°$ for $\rho=0°$ and $\rho=45°$.

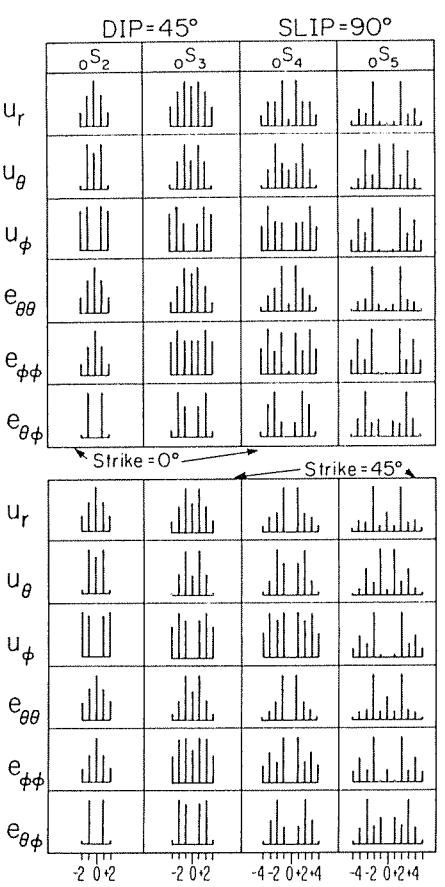

Fig. 5. Spheroidal mode amplitude spectra for a 45° dipping dip slip fault at $\theta_s=30°$, $\phi_s=0°$ observed at $\theta=105°$, $\phi=120°$ for $\rho=0°$ and $\rho=45°$.

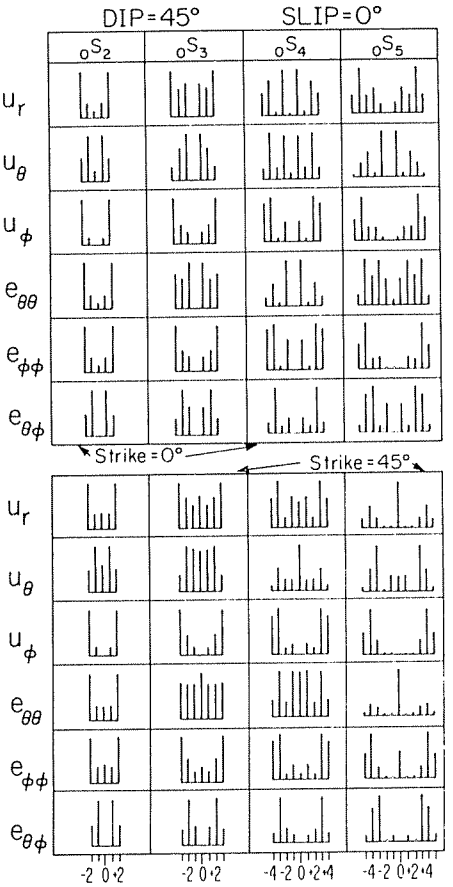

Fig. 6. Spheroidal mode amplitude spectra for a 45° dipping strike slip fault at $\theta_s=30°$, $\phi_s=0°$ observed at $\theta=105°$, $\phi=120°$ for $\rho=0°$ and $\rho=45°$.

spectral amplitudes are equal for the positive and negative ($\pm m$) members of each singlet pair. It is also interesting that the amplitudes depend separately on the colatitude of the source and receiver, rather than only on the separation. In fact, the longitudes have no effect on the amplitude spectra and affect only the phase. (For a spatially finite source, the longitudes will affect the spectral amplitudes through interference, and the $\pm m$ amplitudes will no longer be equal.)

Figures 3–6 show spectra for four basic fault geometries: vertical dip slip, vertical strike slip, 45° dipping dip slip and 45° dipping strike slip. Two cases are shown in each figure. The top halves of the figures show spectra for the case of fault strike, $\rho=0°$ and the bottom halves are for $\rho=45°$. Each half is organized as follows. The columns, from left to right, display the multiplets

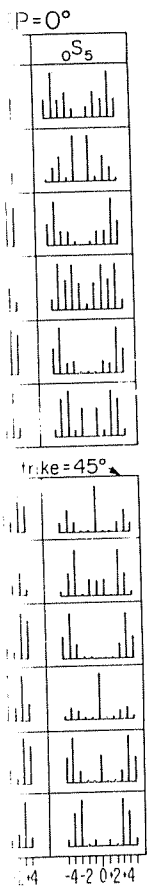

plitude spectra
ip fault at $\theta_s=$
105°, $\phi=120°$

members of
d separately
the separa-
ra and affect
ll affect the
ides will no

vertical dip
e slip. Two
y spectra for
. Each half
he multiplets

$_0S_2$, $_0S_3$, $_0S_4$ and $_0S_5$. The rows, from top to bottom, show the displacement components U_r, U_θ, U_ϕ and strain components $e_{\theta\theta}$, $e_{\phi\phi}$ and $e_{\theta\phi}$. All of the plots were made with the epicenter at $\theta_s=30°$, $\phi_s=0°$ and a receiver at $\theta=105°$, $\phi=120°$. Thus, regardless of the source geometry, several singlets always have low amplitudes in these figures because of the small values of $P_l^m(\cos 105°)$ or its derivatives. Even so, the changes in relative spectral amplitudes at a given receiver site (for which the arguments of the associated Legendre polynomials and their derivatives are fixed) caused by variations in fault parameters are substantial.

In general the effect of varying the fault strike appears to be less significant than that of varying the dip or slip angles. In certain cases though, a change in the strike can cause substantial changes in the spectra. For example, for the 45° dipping strike slip fault with $\rho=0°$ in Fig. 6, the $m=0$ (zonal) singlet is small for all four multiplets. On the other hand, the 45° striking fault has large zonal amplitudes for several components. In fact, the zonal term dominates the U_r component of $_0S_5$, U_θ of $_0S_4$ and $e_{\theta\theta}$ of $_0S_5$, which contrast sharply to the same components for the north striking fault. The change in strike has an even more remarkable effect for Fig. 4, the vertical strike slip fault. The zonal term is identically zero for the north striking fault, but dominates some of the components of the 45° striking fault (e.g. U_r and $e_{\theta\theta}$ of $_0S_5$ and U_θ of $_0S_4$). (It can be seen either intuitively, from the asymmetry of the displacement about the fault with longitude, or formally, from (5.3), that the zonal terms are zero for the north striking strike slip fault.) In Figs. 3 through 6 the 45° striking fault usually has a larger amplitude for the zonal singlet than the north striking fault; of course the amplitude of the zonal singlet is always zero for U_ϕ and $e_{\theta\phi}$. Changes in the strike alter the relative excitation within all of the multiplets in these figures; the 45° dipping slip fault (Fig. 5) is affected least.

The effects of varying the dip and slip directions are even more noticeable. For our four figures this effect stems from the different radiation pattern factors, q_i, listed in Table 2. The q_i in turn affect the polar frame excitation coefficients given by (5.3). Note that for a particular strike (either $\rho=0°$ or 45°), the $_0S_4$ and $_0S_5$ multiplets look similar for the two strike slip faults (Figs. 4 and 6), and that these multiplets are less similar for the dip slip faults (Figs. 3 and 5). The strike-slip pair is quite dissimilar to the dip slip pair. Such generalizations cannot be made for $_0S_2$ and $_0S_3$. For example, for $_0S_2$ the U_r components of the strike slip faults appear similar while the dip slip faults are very different. These effects can be understood in terms of the coefficients in Tables 1 and 2, the rotation matrices and the vector spherical harmonics, but each individual case must be analyzed in detail. For example, $_0S_2$ changes substantially with a change in strike for the vertical dip slip fault (Fig. 3),

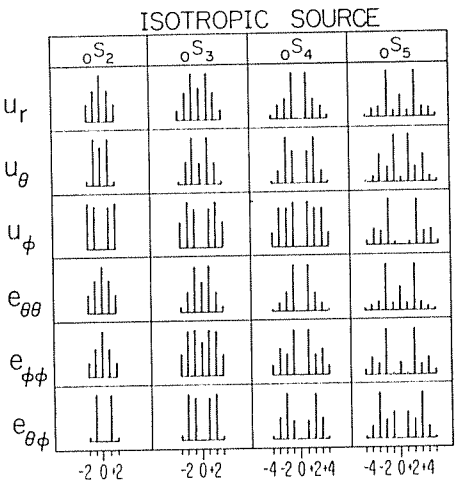

Fig. 7. Spheroidal mode amplitude spectra for an isotropic source at $\theta_s = 30°$, $\phi_s = 0°$ observed at $\theta = 105°$, $\phi = 120°$.

but hardly at all for the 45° dipping dip slip fault (Fig. 5). The reason for this is discussed in detail below.

In Fig. 7 we show the spectra for an "isotropic" point source (e.g. an explosion). The relative spectral amplitudes within a multiplet are obtained from (5.9), (5.12) and (5.13). (It can be seen from (3.3), (3.5) and (5.3) that "fault strike," ρ, has no effect on the spectra.) Note that for ${}_0S_2$ and ${}_0S_3$ the spectra in Fig. 7 are nearly identical to the spectra in Figs. 5a and 5b. Even if the fault dip is reduced to 10° (not shown here) the similarity remains. The explanation of this similarity is as follows. From Table 1 we see that, for ${}_0S_2$ and ${}_0S_3$, K_0 is several hundred times larger than K_1 or K_2. Whenever q_0, the coefficient of K_0 in (5.7), is comparable in magnitude to q_1 and q_2, then the "isotropic" term will dominate the spectra. From Table 2 we see that for the four basic fault geometries only the 45° dipping dip slip fault has $q_0 \neq 0$. Thus the spectra from this fault resemble the isotropic spectra, while the spectra in Figs. 3, 4 and 6 do not.

Thus the spectra from a shallow angle thrust fault closely resemble the spectra from an isotropic source for low order spheroidal modes. In a recent paper (GELLER and STEIN, 1977) we discuss the observational consequences of this similarity. KANAMORI and CIPAR (1974) determined the mechanism of the 1960 Chilean earthquake to be a low angle thrust fault. Due to this particular geometry, PEKERIS *et al.* (1961) were able to match the observed relative spectral amplitudes with an isotropic source model. Spectra from the isotropic source would not have matched the spectra of a pure strike-slip earthquake.

Figures 8–11 show the displacement and strain spectra (the moduli of the appropriate l, m component of $\boldsymbol{B}_{lm}$) for torsional modes ${}_0T_2$–${}_0T_5$, for the same set of fault parameters as for the spheroidal modes. The torsional modes have

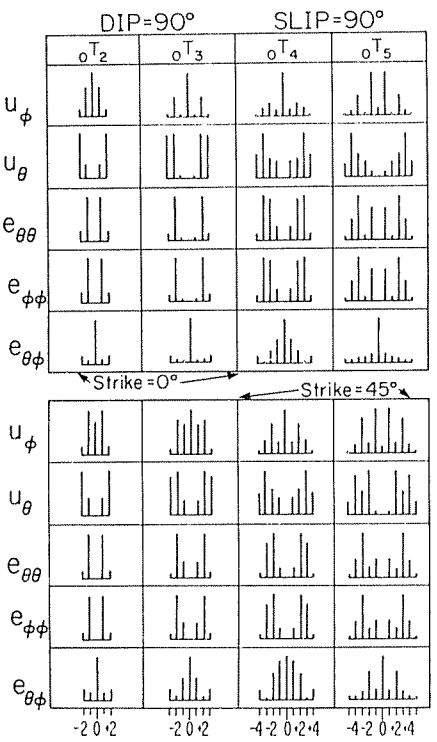

Fig. 8. Torsional mode amplitude spectra for a vertical dip slip fault at $\theta_s=30°$, $\phi_s=0°$ observed at $\theta=105°$, $\phi=120°$ for $\rho=0°$ and $\rho=45°$.

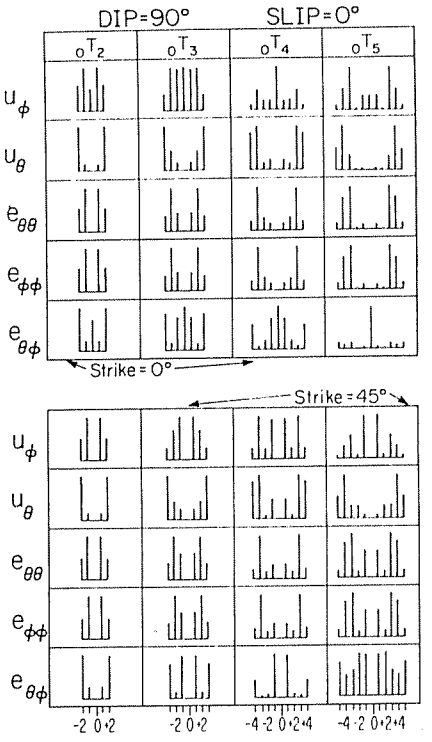

Fig. 9. Torsional mode amplitude spectra for a vertical strike slip fault at $\theta_s=30°$, $\phi_s=0°$ observed at $\theta=105°$, $\phi=120°$ for $\rho=0°$ and $\rho=45°$.

no zonal terms in the source frame, but the zonal singlet in the geographic frame is often excited. A spectacular example is the excitation of the U_ϕ component of $_0T_4$, and the $e_{\theta\phi}$ components of $_0T_5$, by the vertical strike slip fault (Fig. 9). The torsional modes, of course, have no radial displacement component. They also have the property that $e_{\theta\theta}=-e_{\phi\phi}$ since there is no net dilatation. The amplitude spectra of these two strain components are thus identical.

The spectra of the components of $_0T_4$ and $_0T_5$ are generally similar for the two strike slip faults. This resemblance is much weaker for the dip slip faults. For example, $_0T_5$ is similar in Figs. 8 and 10, but $_0T_4$ is quite different. For the two lower angular order modes the spectra of the strike slip faults are generally very similar, while those of the dip slip faults are sometimes similar, but often show substantial differences. An excellent example of this variability can be seen by examining the two displacement components of $_0T_2$ in Figs. 8 and 10—the U_θ components are similar while the U_ϕ components are very different. These same two components show interesting results from a change

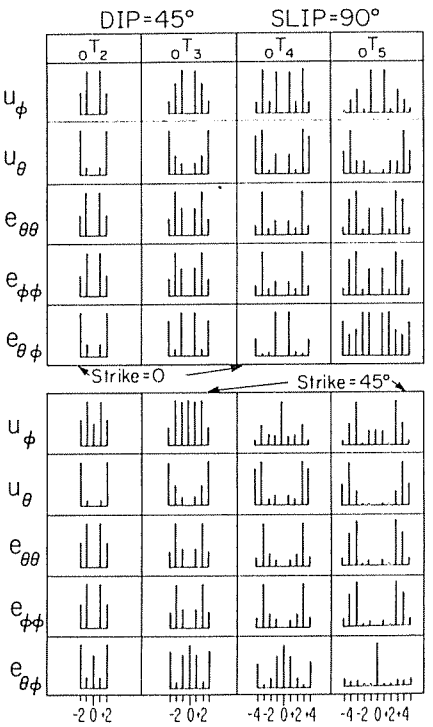

Fig. 10. Torsional mode amplitude spectra for a 45° dipping dip slip fault at $\theta_s=30°$, $\phi_s=0°$ observed at $\theta=105°$, $\phi=120°$ for $\rho=0°$ and $\rho=45°$.

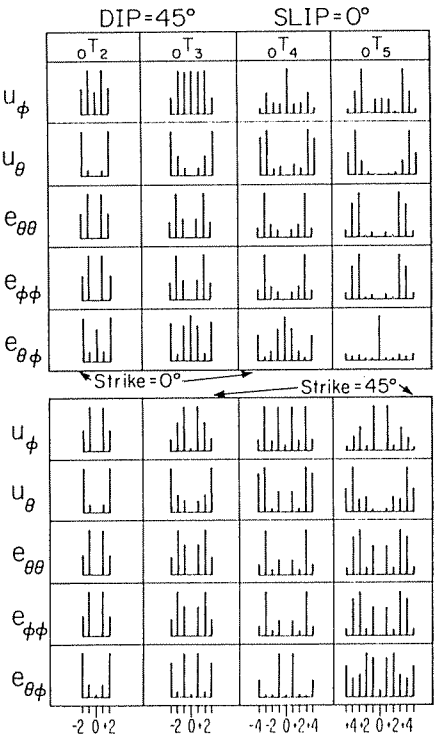

Fig. 11. Torsional mode amplitude spectra for a 45° dipping strike slip fault at $\theta_s=30°$, $\phi_s=0°$ observed at $\theta=105°$, $\phi=120°$ for $\rho=0°$ and $\rho=45°$.

in strike, which can be seen by contrasting the U_ϕ components of $_0T_2$ between the two halves of Fig. 10. As we observed for the spheroidal modes, the 45° striking fault excites the zonal singlet more strongly.

In conclusion, the amplitude spectra for both displacements and strains show a complicated dependence on the fault parameters for a variety of faults. It is not possible to predict the spectra using only the locations of the source and receiver to compute the values of the vector spherical harmonics. The geometric fault parameters (strike, dip and slip) must also be used for a complete synthesis of the relative spectral amplitudes.

7. *Discussion*

Although our derivations are lengthy and somewhat complicated, the results may be easily used to compute the strains and displacements excited by arbitrary faults. The computations are simplified by the separation of the

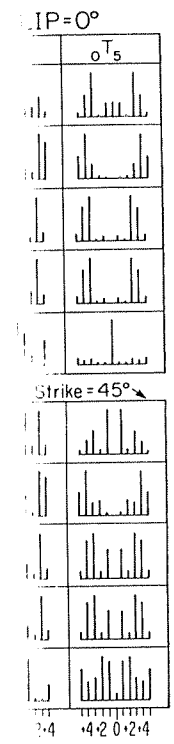

plitude spectra
ip fault at $\theta_s=$
$=105°, \phi=120°$

$_0T_2$ between
des, the 45°

s and strains
iety of faults.
f the source
monics. The
d for a com-

plicated, the
nents excited
uration of the

expressions into factors for five different effects. When any single parameter is changed only part of the results need be recalculated.

The radiation pattern terms q_i and p_i are controlled by the fault dip and slip angles. The Euler angles, and thus the arguments of $D^l_{mk}(R)$, depend on the fault strike and the geographic coordinates of the epicenter. The receiver position provides the arguments of the vector spherical harmonics. The earth's structure controls the radial eigenfunctions and the energy integrals. Finally, the source depth controls the values of $y_i(r_s)$, $\lambda(r_s)$ and $\mu(r_s)$. For computational purposes the earth structure and source depth effects are combined in the source amplitude factors K_0, K_1, K_2 and L_1, L_2.

It is important to note that for a given source-receiver geometry and fault mechanism, the relative amplitudes of the singlet pairs within a multiplet often differs between multiplets, and even between strain and displacement components of the same multiplet. Our figures show that in general, similar patterns are not observed for different multiplets.

Luh and Dziewonski (1976) suggested that certain patterns might persist between multiplets in the excitation of singlets. (Their excitation coefficients roughly correspond to our A_{lm} and D_{lm}.) Their suggestion, which seems to be correct, refers to excitation coefficients which are independent of receiver location. On the other hand, the singlet spectral amplitudes are obtained by multiplying the excitation coefficients by the appropriate components of the vector spherical harmonics. Therefore, since each singlet involves a different spherical harmonic the observed spectral amplitudes are strongly dependent on receiver position. For example, Luh and Dziewonski commented that the prominent $m=\pm 1$ peaks in the strain record of the Chilean earthquake at Isabella (Benioff *et al.*, 1961) might support their suggestion. Since the strain spectrum includes the effect of the receiver location, this similarity is fortuitous. However, in this case the $m=\pm 1$ excitation was so dominant that these lines would be largest at most receivers.

Our synthetic spectra have some implications for the determination of the eigenfrequencies of an "equivalent degenerate earth model" from the actual data. It is not uncommon for a multiplet to be excited such that one pair of singlets (e.g. the U_r or U_ϕ components of $_0S_2^{\pm 2}$ for both 45° dipping strike slip faults in Fig. 6) have much larger amplitudes than the remainder of the multiplet. If the equivalent degenerate central frequency for the multiplet were determined by finding the frequency midway between $_0S_2^2$ and $_0S_2^{-2}$, this estimate would be inaccurate because of the asymmetry of the nondegenerate eigenfrequencies about the unperturbed singlet frequency.

Gilbert (1971) suggests that if sources and receivers are distributed randomly on the earth's surface, then stacking a large number of spectral observations would yield an accurate estimate of the degenerate eigenfrequen-

cies if the averaged amplitudes of the individual singlets are approximately equal. However, the spectral amplitudes are influenced by geometric fault parameters as well as source and receiver locations. Thus, it may also be necessary to stack the spectra for a random sample of fault mechanisms. Failure to do so may lead to systematic errors in estimates of the unperturbed eigenfrequencies of the lowest order modes. Since the present dataset used for eigenfrequency estimation probably does not include a random sample of fault parameters and since it has not been demonstrated that stacking will yield approximately equal singlet amplitudes, further study of this question would be useful.

8. *Conclusions*

We derive expressions for the displacement and strain components of the free oscillations of a laterally homogeneous, rotating and elliptical earth excited by a point double couple. We use the rotation matrix elements $\mathcal{D}^{l}_{mk}(R)$ to derive the excitation of the nondegenerate modes from results developed for the degenerate modes of a nonrotating spherically symmetric earth. Our results are presented in a condensed form suitable for computational use. We show calculations of the excitation of low order modes for a variety of source and receiver locations and for a number of different fault parameters. Our methods allow the synthesis of spectra and time domain records of low order modes for which individual singlets have been observationally resolved. This represents a powerful new tool which may be applied to the study of normal mode amplitude data.

We are deeply indebted to Hiroo Kanamori for his encouragement, patience and advice throughout this study. Jay Melosh offered us several valuable suggestions and loaned us a quantum mechanics book. Dan Novoseller, of the Caltech physics department, supplied us with routines to calculate $d^{l}_{mk}(\beta)$. Peter Luh pointed out to us the exact nature of the excitation coefficients used in his paper. We sincerely thank T. Usami for a thoughtful review and Peter Luh for valuable discussions. Copies of the programs to calculate displacements and strains for torsional and spheroidal modes are available upon request.

Seth Stein was supported by a fellowship from the Fannie and John Hertz Foundation. This research was also supported by National Science Foundation Grants EAR74-22489 and EAR76-14262. This is Contribution Number 2825 of the Division of Geological and Planetary Sciences.

REFERENCES

ABE, K., Determination of seismic moment and energy from the earth's free oscillation, *Phys. Earth Planet. Inter.*, **4**, 49-61, 1970.

ALTERMAN, Z., H. JAROSCH, and C. L. PEKERIS, Oscillations of the earth., *Proc. R. Soc. London*, **A252**, 80-95, 1959.

BACKUS, G. and F. GILBERT, The rotational splitting of the free oscillations of the Earth, *Proc. Nat. Acad. Sci. U.S.A.*, **47**, 362–371, 1961.

BENIOFF, H., F. PRESS and S. SMITH, Excitation of the free oscillations of the earth by earthquakes, *J. Geophys. Res.*, **66**, 675–693, 1961.

BRINK, D. M. and G. R. SATCHLER, *Angular Momentum*, Clarendon Press, Oxford, 1968.

DAHLEN, F. A., The normal modes of a rotating, elliptical Earth, *Geophys. J. R. Astron. Soc.*, **16**, 329–367, 1968.

FUKAO, Y. and K. ABE, Multimode Love waves excited by shallow and deep earthquakes, *Bull. Earthq. Res. Inst. Tokyo Univ.*, **49**, 1–12, 1971.

GELLER, R. J., Body force equivalents for stress drop seismic sources, *Bull. Seism. Soc. Am.*, **66**, 1801–1804, 1976.

GELLER, R. J. and S. STEIN, Split free oscillation amplitudes for the 1960 Chilean and 1964 Alaskan earthquakes, *Bull. Seism. Soc. Am.*, **67**, 651–660, 1977.

GILBERT, F., Excitation of the normal modes of the Earth by earthquake sources, *Geophys. J. R. Astron. Soc.*, **22**, 223–226, 1970.

GILBERT, F., The diagonal sum rule and averaged eigenfrequencies, *Geophys. J. R. Astron. Soc.*, **23**, 119–123, 1971.

KANAMORI, H., Synthesis of long-period surface waves and its application to earthquake source studies—Kurile Islands earthquake of October 13, 1963, *J. Geophys. Res.*, **75**, 5011–5025, 1970a.

KANAMORI, H., The Alaska earthquake of 1964: Radiation of long period surface waves and source mechanism, *J. Geophys. Res.*, **75**, 5029–5040, 1970b.

KANAMORI, H., Focal mechanism of the Tokachi-Oki earthquake of May 16, 1968: Contortion of the lithosphere at a junction of two trenches, *Tectonophysics*, **12**, 1–13, 1971.

KANAMORI, H., Re-examination of the earth's free oscillations excited by the Kamchatka earthquake of November 4, 1952, *Phys. Earth Planet. Int.*, **11**, 216–226, 1976.

KANAMORI, H. and J. J. CIPAR, Focal process of the great Chilean earthquake, May 22, 1960, *Phys. Earth. Planet. Int.*, **9**, 128–136, 1974.

LUH, P. C., Normal modes of a rotating, self-gravitating inhomogenous earth, *Geophys. J. R. Astron. Soc.*, **38**, 187–224, 1974.

LUH, P. C. and A. M. DZIEWONSKI, Theoretical normal-mode spectra of a rotating elliptical earth, *Geophys. J. R. Astron. Soc.*, **45**, 617–645, 1976.

MADARIAGA, R., Toroidal free oscillations of the laterally heterogeneous earth, *Geophys. J. R. Astron. Soc.*, **27**, 81–100, 1972.

MADARIAGA, R. and K. AKI, Spectral splitting of toroidal-free oscillations due to lateral heterogeneity of the earth's structure, *J. Geophys. Res.*, **77**, 4421–4431, 1972.

NESS, N., J. HARRISON and L. SLICHTER, Observations of the free oscillations of the earth, *J. Geophys. Res.*, **66**, 621–629, 1961.

OKAL, E. A., A surface wave investigation of the Gobi-Altai (December 4, 1957) earthquake, *Phys. Earth Planet. Int.*, **12**, 319–328, 1976.

PEKERIS, C. L., Z. ALTERMAN and H. JAROSCH, Rotational multiplets in the spectrum of the earth, *Physiol. Rev.*, **122**, 1692–1700, 1961.

SAITO, M., Excitation of free oscillations and surface waves by a point source in a vertically heterogeneous earth, *J. Geophys. Res.*, **72**, 3689–3699, 1967.

SAITO, M., Theory for the elastic-gravitational oscillation of a laterally heterogeneous earth, *J. Phys. Earth*, **19**, 259–270, 1971.

SATÔ, Y., Transformation of wave functions related to the transformations of coordinate systems, *Bull. Earthq. Res. Inst. Tokyo Univ.*, **28**, 175–217, 1950.

SHIMAZAKI, K., Nemuro-Oki earthquake of June 17, 1973: A lithospheric rebound at the upper half of the interface, *Phys. Earth Planet. Int.*, **9**, 314–327, 1975.

STEIN, S. and R. J. GELLER, Time domain observation and synthesis of split spheroidal and torsional free oscillations of the 1960 Chilean earthquake: preliminary results, *Bull. Seism. Soc. Am.*, submitted 1977.

TAKEUCHI, H. and M. SAITO, Seismic surface waves, *Methods Comput. Phys.*, **11**, 217–295, 1972.

USAMI, T., Effect of horizontal heterogeneity on the torsional oscillation of an elastic sphere, *J. Phys. Earth*, **19**, 175–180, 1971.